



HAL
open science

A Micro-Macro Approach to Modeling Progressive Damage in Composite Structures

T.E. Tay, G. Liu, A. Yudhanto, V.B.C. Tan

► **To cite this version:**

T.E. Tay, G. Liu, A. Yudhanto, V.B.C. Tan. A Micro-Macro Approach to Modeling Progressive Damage in Composite Structures. *International Journal of Damage Mechanics*, 2008, 17 (1), pp.5-28. 10.1177/1056789506067941 . hal-00571162

HAL Id: hal-00571162

<https://hal.science/hal-00571162>

Submitted on 1 Mar 2011

HAL is a multi-disciplinary open access archive for the deposit and dissemination of scientific research documents, whether they are published or not. The documents may come from teaching and research institutions in France or abroad, or from public or private research centers.

L'archive ouverte pluridisciplinaire **HAL**, est destinée au dépôt et à la diffusion de documents scientifiques de niveau recherche, publiés ou non, émanant des établissements d'enseignement et de recherche français ou étrangers, des laboratoires publics ou privés.

A Micro–Macro Approach to Modeling Progressive Damage in Composite Structures

T. E. TAY,* G. LIU, A. YUDHANTO AND V. B. C. TAN
*Department of Mechanical Engineering
National University of Singapore, 9 Engineering Drive 1
Singapore 117576*

ABSTRACT: Modeling progressive damage in composite materials and structures poses considerable challenges because damage is, in general, complex and involves multiple modes such as delamination, transverse cracking, fiber breakage, fiber pullout, etc. Clearly, damage in composites can be investigated at different length scales, ranging from the micromechanical to the macromechanical specimen and structural scales. In this article, a simple but novel finite-element-based method for modeling progressive damage in fiber-reinforced composites is presented. The element-failure method (EFM) is based on the simple idea that the nodal forces of an element of a damaged composite material can be modified to reflect the general state of damage and loading. This has an advantage over the usual material property degradation approaches, i.e., because the stiffness matrix of the element is not changed, computational convergence is theoretically guaranteed, resulting in a robust modeling tool. The EFM, when employed with suitable micromechanics-based failure criteria, may be a practical method for mapping damage initiation and propagation in composite structures. In this article, we present a micromechanical analysis for a new failure criterion called the strain invariant failure theory and the application of the EFM in the modeling of open-hole tension specimens. The micromechanical analysis yields a set of amplification factors, which are used to establish a set of micromechanically enhanced strain invariants for the failure criterion. The effects of material properties and volume fraction on the amplification factors are discussed.

KEY WORDS: progressive damage, multiscale damage, element-failure method, strain invariant failure theory, micromechanical amplification.

*Author to whom correspondence should be addressed. E-mail: mpetayte@nus.edu.sg

INTRODUCTION

DAMAGE PROGRESSION IN composite materials and structures is, in general, very complicated and involves multiple failure modes, such as fiber breakage, fiber pullout, delamination between plies, matrix cracking, fiber–matrix debonding, etc. Modeling the damage process accurately poses a very difficult problem because these mechanisms clearly operate at various length scales (Tay, 2003). However, if more rational design and damage tolerance approaches are to be developed for composite structures, it becomes necessary to develop engineering tools that will enable analysts to model damage and its propagation. At the micromechanics scale, the fibers may be modeled individually and microcracks introduced (Mahishi, 1986). However, the large variations in local fiber distribution and possible flaw sizes quickly renders such models impractical, and invariably, simplifications and idealizations are introduced in the form of representative volume elements (RVE) to make the problem more tractable. The goal of many RVE analyses is to obtain some form of weighted or effective composite property or behavior so that it may be used in constitutive stress–strain relations. Furthermore, it is neither practical nor desirable to model explicitly the very numerous microcracks often observed in damaged composite materials under the microscope. At the macromechanical level of the effective constitutive relations of the damaged material, there have been significant strides in the development of damage mechanics (Cheng and Chen, 2006; Chow et al., 1993; Ju et al., 2006; Paulino et al., 2006; Talreja, 1994). In most damage mechanics approaches, the crucial components are the damage variables, which are sometimes obtained phenomenologically. In a sense, the traditional continuum damage mechanics approach may be viewed as part of the class of methodology whereby damage is modeled by degradation of selective elastic or mechanical properties. This material property degradation method (MPDM) (Camanho and Matthews, 1999; Shokrieh and Lessard, 2000; Tserpes et al., 2001) essentially involves directly reducing the values of certain material properties in the constitutive relations when and if damage or failure is determined. The severity of damage may be characterized by damage evolution laws, which are typically determined through damage mechanics. However, a drawback of this approach is that, by reducing the material properties, there is a possibility that the stiffness matrix of the finite element (FE) may inadvertently become ill-conditioned so that convergence to a solution is not always assured. For a conservative analysis, it is usual to set the values of certain material properties to zero when damage or failure is assumed. For example, if failure is determined to have occurred in the fiber direction (as in the breaking of fibers in tension), the fiber-direction Young’s modulus E_{11} may be set to zero.

However, while not explicitly stated in most published literature, in practice, the material stiffness properties (typically the elastic moduli) are sometimes not set to exactly zero but to a certain (often arbitrarily) small percentage of the original value in order to overcome computational difficulties. Another issue involves deciding which of the many material properties to degrade. For example, if transverse cracking or failure is predicted in a composite, it is not clear if only the transverse Young's modulus E_{22} or the in-plane shear modulus G_{12} as well should be set to zero; additionally, the effect on the Poisson's ratios ν_{12} and ν_{21} is neither obvious nor easily determined. The MPDM is popularly used in laminated-plate and laminated-shell FE codes with failure criteria such as the Tsai–Wu tensor theory, because it is convenient to set to zero the material property values in lamination theory. Examples of application of the Tsai–Wu and other failure theories in progressive damage in composite structures can be found in Ochoa and Engblom (1987), Kim et al. (1996), and Wofford and Hyer (2005). However, the application of MPDM in three-dimensional (3D) problems where delaminations and interactions with numerous damage mechanisms are significant, may be cumbersome. At the moment, it is still very difficult to translate information from a micromechanical analysis to guide the development of modified constitutive relations for damaged composite materials. If this can be achieved, the modeling of damage at the components and structures level, supported by the micromechanics of failure and damage, should result in greater accuracy.

In this article, a novel FE-based element-failure method (EFM) is proposed for the modeling of damage in composite structures, in which only the nodal forces are changed to reflect changes in the stress-bearing capability of the damaged material. Because the stiffness matrix remains unaltered, there is no similar computational problem associated with the MPDM. Another consequence is that there should be savings in computational effort since no reformulation of the stiffness matrix with damage progression is involved; each change in the damage state is modeled by appropriately modifying the nodal forces only. Moreover, a new micromechanics-based failure theory, recently proposed by Gosse and Christensen (Gosse and Christensen, 2001; Gosse, 2002), is used together with the EFM to determine damage initiation and propagation. Called the strain invariant failure theory (SIFT), a unique feature of this failure theory is that information at the micromechanical scale is extracted from micromechanical FE block analyses to amplify strain invariant quantities, which are, in turn, used as criteria to determine failure. In combination with a simple nodal force modification scheme, the SIFT–EFM approach enables the modeling of damage progression in composite

structures that takes into account mechanisms that bridge micro and macro length scales.

The paper first describes the concept and implementation of the EFM, followed by the SIFT. It should be noted that, while we have chosen SIFT for the work reported herein, EFM may in general be used with any appropriate failure theory. Indeed, in an earlier work by the authors (Tay et al., 2003), the Tsai–Wu failure criterion (Tsai, 1992) was used with EFM in a plane strain analysis to predict the pattern of delamination growth by low-velocity impact on composite laminates. However, the Tsai–Wu failure criterion (and some of the other more established failure criteria) is best known for application in essentially plane stress analyses involving the classical-lamination theory (CLT) of laminated plates. Its extension to the more general 3D cases is considerably more complex, and it is difficult to determine the parameters that will ensure closed or admissible failure envelopes in the six-component stress or strain space. Although plane stress analyses significantly simplifies matters and may be sufficient for many design purposes, there is growing realization that damage and delamination in composite structures are truly 3D events with the need for appropriate analytical and modeling tools (Tay, 2003). SIFT is selected partly because it offers a fully 3D theory with inherent micromechanical features. There are other new micromechanics-based failure theories; an example is the so-called multicontinuum failure theory developed by Mayes and Hansen (2001).

This article describes SIFT–EFM’s implementation in a 3D implicit FE code and its application in open-hole tension of composite laminates. The damage maps of several cases are shown.

CONCEPT OF THE EFM

The idea and assumption of EFM is that the effects of damage on the mechanical behavior can be essentially described by the effective nodal forces of an FE. It was first developed for dynamic fracture in metals (Beissel et al., 1998), but the modified EFM was used for impact damage in fiber-reinforced composites (Tay et al., 2003). The manner by which these effects due to damage translate to the effective nodal forces will, in general, depend upon the damage evolution law appropriate for the local mode of damage experienced by the composite material, as well as on the FE formulation. Traditionally, when damage is assumed to have occurred within an element of a material, the stiffness matrix of the element is altered to reflect the damaged state. One is able to develop explicit

relations between the nodal forces and the elastic stiffnesses of an FE as follows.

The force–stiffness relation for a finite element is given by

$$\mathbf{K}\mathbf{u} = \mathbf{f} \quad (1)$$

where \mathbf{u} is the vector of nodal displacements, \mathbf{f} the vector of nodal forces, and \mathbf{K} the elemental stiffness matrix of undamaged material, integrated over the domain Ω ,

$$\mathbf{K} = \int_{\Omega} \mathbf{B}^T \mathbf{C} \mathbf{B} \, \partial\Omega. \quad (2)$$

For 2D plane strain or plane stress problems, elements of the material stiffness matrix C_{ij} are defined for $i, j = 1, 2, 6$. Although equations for 2D FE are used for illustrative purposes, the extension to 3D FE is similar and straightforward.

The matrix \mathbf{B} is defined as

$$\mathbf{B} = \begin{bmatrix} N_{1,x} & 0 & N_{2,x} & 0 & \cdots & N_{m,x} & 0 \\ 0 & N_{1,y} & 0 & N_{2,y} & \cdots & 0 & N_{m,y} \\ N_{1,y} & N_{1,x} & N_{2,y} & N_{2,x} & \cdots & N_{m,y} & N_{m,x} \end{bmatrix} \quad (3)$$

where m is the number of nodes for the element, and $N_{i,x} = (\partial N_i / \partial x)$ and $N_{i,y} = (\partial N_i / \partial y)$ are the derivatives of the shape functions N_i with respect to the global x and y coordinates, respectively.

The elemental stiffness matrix \mathbf{K} can be written as

$$\mathbf{K} = \begin{bmatrix} \mathbf{K}_{11} & \mathbf{K}_{12} & \cdots & \mathbf{K}_{1m} \\ & \mathbf{K}_{22} & \cdots & \mathbf{K}_{2m} \\ & & \ddots & \vdots \\ \text{symm.} & & & \mathbf{K}_{mm} \end{bmatrix} \quad (4)$$

where \mathbf{K}_{ij} is a matrix of the form

$$\mathbf{K}_{ij} = \begin{bmatrix} C_{11} \int_{\Omega} N_{i,x} N_{j,x} \, \partial\Omega + C_{66} \int_{\Omega} N_{i,y} N_{j,y} \, \partial\Omega & C_{12} \int_{\Omega} N_{i,x} N_{j,y} \, \partial\Omega + C_{66} \int_{\Omega} N_{i,y} N_{j,x} \, \partial\Omega \\ C_{12} \int_{\Omega} N_{i,y} N_{j,x} \, \partial\Omega + C_{66} \int_{\Omega} N_{i,x} N_{j,y} \, \partial\Omega & C_{22} \int_{\Omega} N_{i,y} N_{j,y} \, \partial\Omega + C_{66} \int_{\Omega} N_{i,x} N_{j,x} \, \partial\Omega \end{bmatrix},$$

for $i, j = 1, 2, \dots, m$.

(5)

Substituting Equations (2) through (5) into Equation (1), the x and y components of the nodal force for node i can be explicitly written as

$$\begin{aligned}
 f_{xi} &= C_{11} \int_{\Omega} N_{i,x} \left(\sum_j^m N_{j,x} u_{xj} \right) \partial\Omega \\
 &+ C_{12} \int_{\Omega} N_{i,x} \left(\sum_j^m N_{j,y} u_{yj} \right) \partial\Omega \\
 &+ C_{66} \int_{\Omega} N_{i,y} \left(\sum_j^m N_{j,y} u_{xj} + \sum_j^m N_{j,x} u_{yj} \right) \partial\Omega
 \end{aligned} \tag{6}$$

and

$$\begin{aligned}
 f_{yi} &= C_{12} \int_{\Omega} N_{i,y} \left(\sum_j^m N_{j,x} u_{xj} \right) \partial\Omega \\
 &+ C_{22} \int_{\Omega} N_{i,y} \left(\sum_j^m N_{j,y} u_{yj} \right) \partial\Omega \\
 &+ C_{66} \int_{\Omega} N_{i,x} \left(\sum_j^m N_{j,y} u_{xj} + \sum_j^m N_{j,x} u_{yj} \right) \partial\Omega.
 \end{aligned} \tag{7}$$

Equations (6) and (7) show the relationship between nodal forces and the material stiffness properties. It is clear that for every change in the stiffness coefficients C_{ij} , there are corresponding changes in the nodal forces. The EFM, however, works through the direct manipulation of the nodal forces. While it is possible to work out the required nodal force modifications with any given set of changes in material stiffness properties, the reverse is not generally true. In other words, a set of changes to the nodal forces may not translate to a set of identifiable changes in material stiffness properties. A detailed comparison with material degradation methods and comparison with the solution for a central cracked panel are given in Tay et al. (2005). It was shown that the EFM is a more general method than the material degradation method.

Consider an FE of an undamaged composite material (Figure 1a) experiencing a set of nodal forces, which have been obtained from the FE solution of the problem. On the other hand, in an FE containing damaged material, the load-carrying capacity of the FE will be compromised, very likely in a directionally and spatially dependent manner. If much of the damage consists of transverse matrix microcracks, it is reasonable to assume that the FE will have reduced load-bearing capacity in the direction transverse to the fibers (Figure 1b). In conventional MPDMs, this reduction

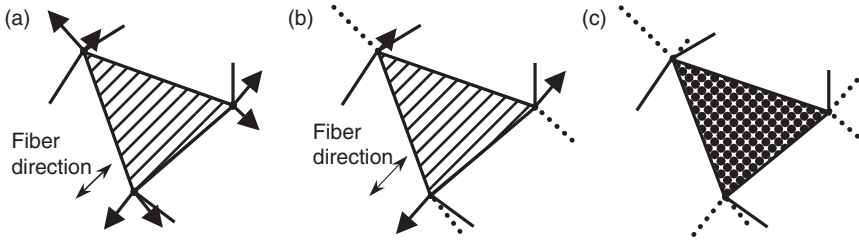


Figure 1. (a) FE of undamaged composite with internal nodal forces. (b) FE of composite with transverse matrix cracks, components of internal nodal forces transverse to fiber direction are modified; and (c) completely failed or fractured element. All net internal nodal forces of adjacent elements are zeroed.

is achieved by reducing or zeroing certain pertinent material stiffness properties of the damaged FE. In the EFM, however, the reduction is effected by applying a set of external nodal forces such that the net internal nodal forces of elements adjacent to the damaged element are reduced or zeroed [the latter if complete failure or fracture is implied (Figure 1c)]. The decision whether to fail an element is guided by a suitable failure theory, and in each step, only one or two elements are failed at a time. The required set of applied nodal forces to achieve the reduction within each step is determined by successive iterations until the net internal nodal forces (residuals) of the adjacent elements converge to the desired values. Typically, less than 200 iterations are required and convergence is guaranteed. Note that it is not the internal nodal forces of the damaged element that is zeroed [for the case of complete failure (Figure 1c)], but the net internal nodal forces of adjacent elements. Thus, the ‘stresses’ within the failed element no longer have physical meaning, although compatibility may be preserved. This process leaves the original (undamaged) material stiffness properties unchanged, and is thus computationally efficient as every step and iteration is simply an analysis with the updated set of applied nodal forces. For this reason, it may also be called the nodal force modification method. Hence, no reformulation of the FE stiffness matrix is necessary.

IMPLEMENTATION OF THE EFM

The EFM has been implemented in an in-house 3D implicit FE code. Since the method merely involves nodal force modification, it can also be readily implemented in commercial FE codes. However, a commercial general-purpose code was not used to implement EFM because it was not possible to over-ride the internal computational housekeeping associated with each step of nodal force modification, which would unnecessarily

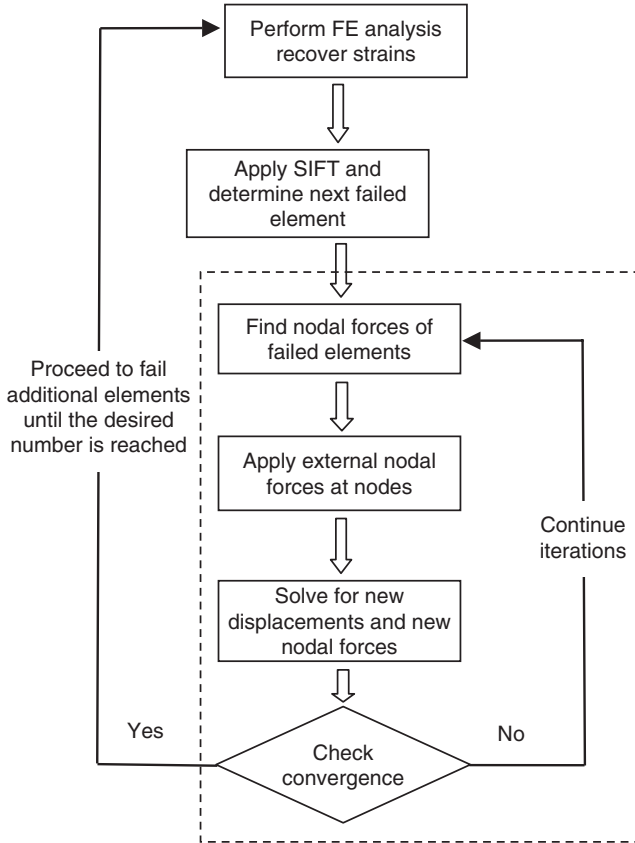


Figure 2. Implementation flow chart of EFM.

increase the computational time. Hence, it was necessary to validate the in-house codes by comparing their solutions for simple problems without damage with those of the general purpose FE code Abaqus.

Figure 2 is the implementation flowchart of the EFM. It begins with a straightforward linear elastic FE analysis of the problem. The solution in terms of strains is fed into the portion of the program that deals with determining failure; in this case, the program uses SIFT. Within this subroutine, the strains are amplified through amplification factors predetermined from micromechanical block analyses, and the three strain invariants are calculated. These are, in turn, compared with their critical values, and failure is determined when any one of them reaches its critical value. A more complete description of SIFT and method of strain amplification is reserved for a subsequent section.

The analysis then proceeds to the part of the program that deals with nodal force modification, where the appropriate scheme is applied to all the nodes of the failed element. For the moment, a simple nodal force modification scheme is employed; it zeroes the components of the internal nodal forces that are transverse to the fiber direction. This assumes that the dominant damage mode at the micromechanics level is transverse microcracking, which could, in reality, be various combinations of microfractures within the matrix material and fiber–matrix debonding. This assumption is considered reasonable and conservative for initial-stage damage or damage that is not yet very severe or extensive.

However, it is possible that an already partially failed element (with mainly matrix microcracks and/or fiber–matrix microdebonds) may subsequently fail completely (by local fiber rupture). It is, therefore, necessary to develop a criterion to determine when partially failed elements may lose all load-bearing capability. A very simple criterion is to use the ultimate failure strain of neat carbon fibers. The rationale is that when extensive matrix microcracks have already occurred, the fibers, while still able to carry some load, are no longer as constrained locally by the surrounding matrix material as before. The ultimate failure strain of fibers, however, is a property that may be dependent upon the length of fiber tested. Nevertheless, recent tests of woven foldable composite structures (Yee and Pellegrino, 2005) show that the maximum bending strains (in the fiber direction) of T300 fiber composites range from 1.9 to 2.8%. A value of 1.9% for the ultimate failure strain of IM7 fiber is reported by Kollar and Springer (2003). The value for the fiber's ultimate failure strain $\epsilon_{\text{fiber}}^{\text{ult}}$ of 1.9% is used later in the section titled '3D implicit FE analysis of damage in open-hole tension laminates' to determine the ultimate failure loads of two open-hole tension composite laminates, which compare reasonably well with experiment. If fiber failure is detected, then all components of the in-plane nodal forces are modified, and the situation for the failed element resembles the state in Figure 1c.

In general, whenever an element is deemed to have failed, nodal forces transverse to the fiber direction are modified. Furthermore, if the partially failed element is found to have strains in the fiber direction exceeding 1.9%, additional nodal force modification is applied to the element in the fiber direction. The external forces are applied until the desired residual internal nodal force values (in this case, zero) are reached. This process takes typically a few iterations, but convergence is always assured. After convergence has been achieved, the program, guided by the failure theory, searches out the next element that has failed and performs the nodal modification for that element. If and when no elements are deemed to have failed, the applied load or displacement for the structure is increased until failure is again predicted.

It is found that in the open-hole tension cases studied here, the situation whereby elements have completely failed (Figure 1c) only occurs in significant numbers very close to the ultimate load. In other words, while SIFT predicts mainly transverse cracking and delamination, the load drop due to these damages, while significant, is usually not as large as those when elements start to fail completely (i.e., also along the fiber direction) in large numbers. When the latter happens, ultimate failure is imminent.

THE STRAIN INVARIANT FAILURE THEORY (SIFT)

In this section, a description of the new strain invariant failure theory (SIFT) is given. The EFM, of course, may be used with other failure theories, but SIFT is chosen because it is fully 3D. Recently proposed by Gosse and Christensen (Gosse and Christensen, 2001; Gosse, 2002), the theory determines if failure has occurred by considering the criticality of three strain invariant values, which have been ‘amplified’ through micromechanical analysis. The procedure is more fully described later, but essentially, the strain components from the homogenous FE solution are amplified with thermo-mechanical amplification factors extracted from unit cell FE micromechanical models before the invariants are calculated.

The first of the invariants is J_1 , defined by

$$J_1 = \varepsilon_{xx} + \varepsilon_{yy} + \varepsilon_{zz} \quad (8)$$

where ε_{xx} , ε_{yy} , ε_{zz} , ε_{xy} , ε_{yz} , and ε_{xz} are the six components of the strain vector in general Cartesian coordinates. Where distortional deformation is significant, a criterion based on the second deviatoric strain invariant may be more useful.

The second deviatoric strain invariant J'_2 is defined by

$$J'_2 = \frac{1}{6} \left[(\varepsilon_{xx} - \varepsilon_{yy})^2 + (\varepsilon_{yy} - \varepsilon_{zz})^2 + (\varepsilon_{xx} - \varepsilon_{zz})^2 \right] - \frac{1}{4} \left(\varepsilon_{xy}^2 + \varepsilon_{yz}^2 + \varepsilon_{xz}^2 \right). \quad (9)$$

SIFT employs the von Mises (or equivalent) strain, which is related to the second deviatoric strain invariant by

$$\varepsilon_{vm} = \sqrt{3J'_2}. \quad (10)$$

These strain invariants are amplified through the use of representative micromechanical blocks, whereby individual fiber and matrix are modeled by 3D FEs (Figure 3). Three fiber arrangements or arrays are considered: square; hexagonal; and diamond. The diamond arrangement is, in fact, the same as the square, but rotated through a 45° angle. These representative

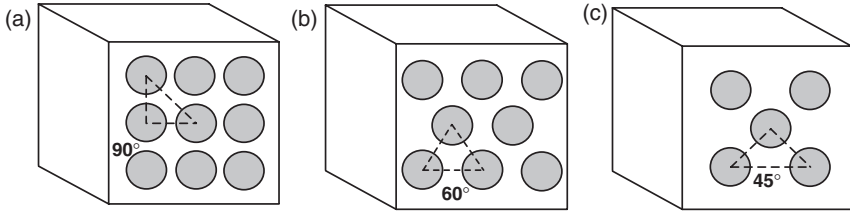


Figure 3. Micromechanical blocks with (a) square, (b) hexagonal, and (c) diamond packing arrays.

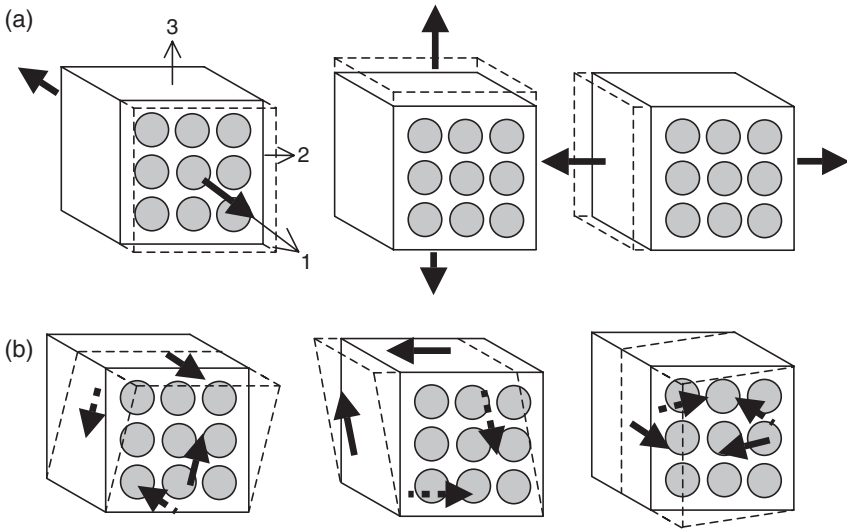


Figure 4. (a) Prescribed normal displacements and (b) prescribed shear deformations.

micromechanical blocks are given prescribed unit displacements in three cases of normal and three cases of shear deformations. For example, in order to obtain strain amplification factors for prescribed displacement in the fiber (labeled 1) direction for one of the faces, the model is constrained in the other five faces (Figure 4a). The procedure is repeated each time in order to obtain strain amplification factors for displacements in the other two orthogonal (labeled 2 and 3) directions. Similarly, for shear deformations, the prescribed shear strain is applied in each of the three directions (Figure 4b). The local micromechanical strains are extracted from various positions within the model (Figure 5) and normalized with respect to the prescribed strain. In addition to the aforementioned mechanical amplification factors, the so-called thermo-mechanical amplification

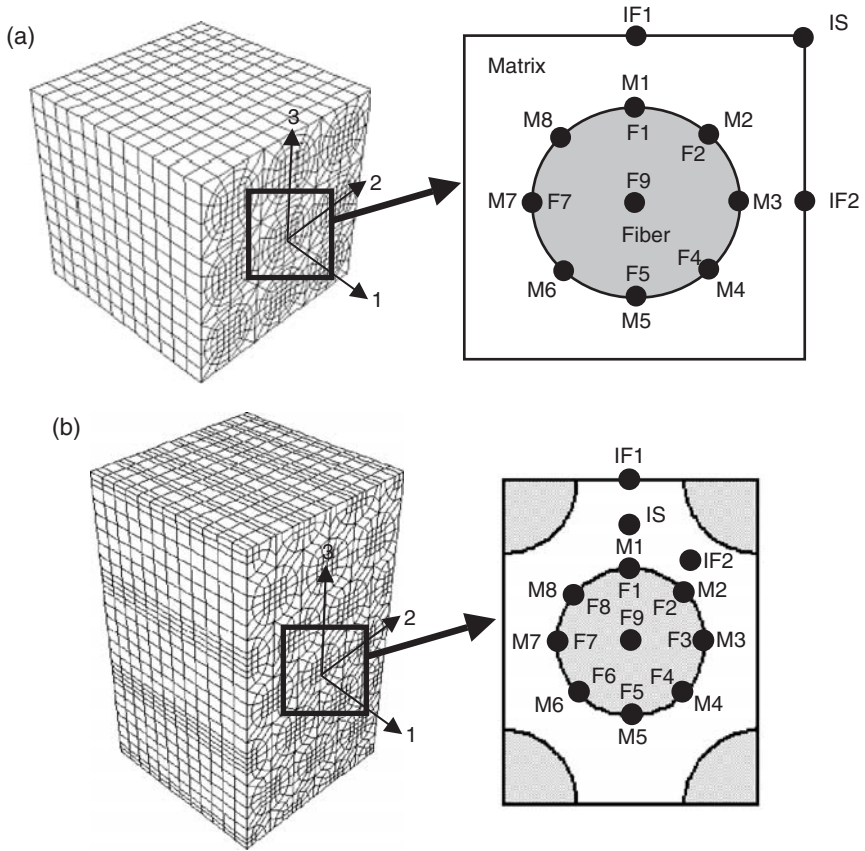


Figure 5. Locations for the extraction of amplification factors within the micromechanical block models: (a) square array and (b) hexagonal array.

factors may be obtained by constraining all the faces from expansion and performing a thermo-mechanical analysis by prescribing a unit temperature differential above the strain-free temperature. In the subsequent analysis, thermal effects are included by prescribing a ΔT of 155°C , which is between the cure or stress-free temperature of 180°C and the use temperature of 25°C .

The locations chosen for the extraction of local amplification factors are shown in Figure 5a for the square array model and Figure 5b for the hexagonal array model. The points F1 through F8 are located at the fiber-matrix interface and are for values of amplification factors computed using fiber properties, while points M1 through M8, also located at the same positions along the fiber-matrix interface, are for values of amplification

Table 1. Fiber and epoxy elastic properties used in micromechanical block models.

	IM7 carbon fiber	S-glass fiber		Epoxy
E_{f1}	303 GPa	85.50 GPa	E_m	3.31 GPa
E_{f2}	15.2 GPa	85.50 GPa		
E_{f3}	15.2 GPa	85.50 GPa		
ν_{f12}	0.2	0.2	ν_m	0.35
ν_{f13}	0.2	0.2		
ν_{f23}	0.2	0.2		
G_{f12}	9.65 GPa	35.65 GPa		
G_{f13}	9.65 GPa	35.65 GPa		
G_{f23}	6.32 GPa	35.65 GPa		
α_{f1}	0	$5.04 \times 10^{-6}/^\circ\text{C}$	α_m	$5.76 \times 10^{-5}/^\circ\text{C}$
α_{f2}	$8.28 \times 10^{-6}/^\circ\text{C}$	$5.04 \times 10^{-6}/^\circ\text{C}$		
α_{f3}	$8.28 \times 10^{-6}/^\circ\text{C}$	$5.04 \times 10^{-6}/^\circ\text{C}$		

factors computed with matrix properties. The point F9 is located at the center of the (assumed circular) fiber, IF1 and IF2 are inter-fiber positions and IS corresponds to the interstitial position. The total number of locations is therefore 20. There are six mechanical and six thermo-mechanical strain amplification factors for each position; since there are 20 positions and three fiber arrangements, the total number of amplification factors is 720 (i.e., $12 \times 20 \times 3$). It should be noted that for a given matrix and fiber material system, the suite of micromechanical block analyses need only be performed once; the resulting amplification factors are stored in a look-up table or subroutine. The output of strains from a macro-FE analysis is efficiently amplified through this look-up subroutine before the strain invariant values are calculated and compared with the corresponding critical values. The amplification factors for carbon fiber–epoxy system used in all the analyses reported in this article were obtained from Gosse (Kim et al., 1996) and coded in a look-up subroutine. However, the amplification factors have been independently verified by the authors, who performed the micromechanical FE block analyses. The matrix and carbon fiber (IM7) material properties are given in Table 1. The subscripts m and f refer to matrix and fiber, respectively; the subscript 1 indicates the axial fiber direction, the subscripts 2 and 3 the transverse directions. The material properties for IM7 and epoxy are obtained from Ha (2002), Gosse and Christensen (2001), and Gosse (2002). The properties for S-glass fiber in the table, used in the subsequent section on the effect of changing materials on the amplification factors, are derived from Gibson (1994).

The first strain invariant J_1 (Equation (8)) is calculated with strains amplified only at the IF1, IF2, and IS positions within the matrix material in

the micromechanical block. It is generally believed that J_1 -driven failure is dominated by volumetric changes in the matrix material. On the other hand, the von Mises strain (Equation (10)) may be amplified with factors not only within the matrix material (IF1, IF2, IS, and M1 through M8), but also within the fiber and fiber–matrix interface (F1 through F9). We designate the superscript m for the former case to denote ‘matrix’ (i.e., ε_{vm}^m) and the superscript f for the latter case to denote ‘fiber’ (i.e., ε_{vm}^f). SIFT states that failure occurs when any one of the three strain invariant values reaches its respective critical values (i.e., J_{1Crit} , ε_{vmCrit}^m , and ε_{vmCrit}^f), which are determined from the analysis of coupon tests of composite laminates with various lay-ups (Gosse and Christensen, 2001; Gosse, 2002). It is clear from the foregoing that for each failure prediction, it is possible not only to determine the invariant that has become critical, but also the position within the micromechanical block model where this has occurred.

It should also be noted that the third critical SIFT criterion ε_{vmCrit}^f is an effective property, obtained through the testing of unnotched 0° unidirectional and $[10^\circ/-10^\circ]_{ns}$ laminates in tension (Gosse, 2002). The critical values of the strain invariants used in the work reported here are derived from the experimental data of Gosse (2002) and given in Table 2. In fact, all the SIFT criteria are effective properties of the composite and not only of dry fibers or pure polymers. Analysis of extensive test data have shown that the failure of fibers within a 0° laminate (unnotched tension) and the failure of fibers in a $[10^\circ/-10^\circ]_{ns}$ laminate (also unnotched tension) occur near a common ε_{vm}^f . Since the extraction of the SIFT invariants is done through the micromechanical block models, we hypothesize that the criterion ε_{vm}^f (at the locations along the fiber–matrix interface) incorporates not just the behavior of the fiber phase, but also the interfacial behavior (or at least the matrix phase very near the fiber). Viewed in this way, ε_{vm}^f is not just a fiber-only strength value. This third invariant can become critical if the fiber material or if the matrix material very close to the fiber is

Table 2. Material properties of carbon–epoxy composite used in OHT FE models.

Modulus in fiber direction E_1 (GPa)	161.3
Transverse moduli $E_2 = E_3$ (GPa)	8.3
Shear moduli $G_{12} = G_{13}$ (GPa)	5.16
Shear modulus G_{23} (GPa)	3.38
Thermal expansion coefficient in fiber direction α_1 ($^\circ\text{C}$)	0.01×10^{-6}
Thermal expansion coefficients in transverse direction $\alpha_2 = \alpha_3$ ($^\circ\text{C}$)	32.7×10^{-6}
Critical invariant J_{1Crit}	0.0274
Critical invariant ε_{vmCrit}^m	0.103
Critical invariant ε_{vmCrit}^f	0.0182

compromised or both. However, it is very difficult to test this hypothesis directly.

The micromechanical block models described in the preceding text contain idealized fiber arrangements. In reality, the fibers are arranged in random order. The question, therefore, arises as to whether it is acceptable to use idealized arrangements. A recent article by Jin et al. (2007) addresses the issue of random fiber arrangement in micromechanical block models, utilizing statistical methods to obtain strain amplification factors. They actually built micromechanical block models with large numbers of fibers arranged randomly and found that the mean values of the strain amplification factors for random distributions more closely resemble the values from the hexagonal arrangements. For the moment, this is a subtopic for further study. The authors aim to incorporate amplification factors derived from block models with random fiber arrangements in future analyses.

EFFECTS OF CHANGING VOLUME FRACTIONS AND MATERIALS

The maximum amplification factors computed from the micromechanical block models with three different volume fractions are shown in Table 3 for the square array and Table 4 for the hexagonal array. In each table, the three orthogonal directions of tensile loading are denoted by ‘Dir-1’, ‘Dir-2’ and ‘Dir-3’, while the shear loadings are given by ‘Dir-12’, ‘Dir-13’, and ‘Dir-23’. Clearly, due to rotational symmetry, the case for Dir-2 yields the same results for Dir-3, and for the square array model, Dir-12 produces the same results for Dir-13. The maximum or highest values of amplification factors are shown in bold fonts, while the next highest are shown below the highest in italics. Similarly, the locations of the occurrence of the maximum amplification factors are denoted by bold fonts, and the locations of the next highest by italic fonts.

We see that in loading modes normal to the direction of the fibers, the maximum amplification factors appear in the inter-fiber regions (IF1 and IF2), suggesting possible failure in the matrix material, although the next highest values occur at the fiber–matrix interface (M1, M5, M3, and M7). For shear cases in the 1–2 and 1–3 planes, amplification factors for the highest and the next highest values are extremely close, especially for the fiber volume $V_f=60\%$ case. This suggests that failure in the case of pure shear is almost equally likely to occur in the matrix (IF1 and IF2) as in the fiber–matrix interface (M1, M5, M3, and M7). For the case of shear across the fibers in the 2–3 plane, failure in the matrix is more likely to be in the interstitial position (IS) although failure in the fiber–matrix interface may

Table 3. Effect of fiber volume fraction V_f on amplification factors in square array model (Figures in bold are maximum values; figures in italics are the next highest values. Positions are marked in Figure 5).

Fiber volume fraction	Dir-1	Dir-2	Dir-3	Dir-12	Dir-13	Dir-23
$V_f = 50\%$						
Maximum amplification factor	1.0	2.494	2.494	3.308	3.308	2.280
Position	All points	<i>IF1</i>	<i>IF2</i>	<i>IF1</i>	<i>IF2</i>	<i>IS</i>
		<i>M1, M5</i>	<i>M3, M7</i>	<i>M1, M5</i>	<i>M3, M7</i>	<i>M1, M3, M5, M7</i>
$V_f = 60\%$						
Maximum amplification factor	1.0	2.897	2.897	4.662	4.662	2.623
Position	All points	<i>IF1</i>	<i>IF2</i>	M1, M5	M3, M7	<i>IS</i>
		<i>M1, M5</i>	<i>M3, M7</i>	<i>IF1</i>	<i>IF2</i>	<i>M1, M3, M5, M7</i>
$V_f = 70\%$						
Maximum amplification factor	1.0	3.156	3.156	7.502	7.502	3.904
Position	All points	<i>IF1</i>	<i>IF2</i>	<i>IF1</i>	<i>IF2</i>	M1, M3, M5, M7
		<i>M1, M5</i>	<i>M3, M7</i>	<i>M1, M5</i>	<i>M3, M7</i>	<i>IF1, IF2</i>

still occur. At the high volume fraction of $V_f = 70\%$, the preferred failure site appears to switch to the interface region from the interstitial position. Generally, maximum amplification factors increase with increasing fiber volume fraction. However, this does not mean that resin-rich composites are necessarily more resistant to damage progression, because the macroscopic composite elastic properties will also change with volume fraction and the critical invariants will also very likely be functions of volume fraction.

The effect of changing the fiber material from that of carbon IM7 to S-glass is shown in Table 5 (for square array) and Table 6 (for hexagonal array). The fiber volume in each table is kept at 60% for comparison. The properties of the fibers and epoxy are given in Table 2.

THREE-DIMENSIONAL IMPLICIT FE ANALYSIS OF DAMAGE IN OPEN-HOLE TENSION LAMINATES

A 3D implicit EFM code (with SIFT) was written and applied to the analysis of open-hole composite laminates under uniform remote tension loading. Damage progression for a carbon–epoxy cross-ply laminate with a stacking sequence $[0_3/90_4]_s$ is shown in Figure 6a and b. The diameter of the hole is 12.7 mm, and the width of the plate is 76.2 mm. The macroscopic

Table 4. Effect of fiber volume fraction V_f on amplification factors in hexagonal array model (Figures in bold are maximum values; figures in italics are the next highest values. Positions are marked in Figure 5).

Fiber volume fraction	Dir-1	Dir-2	Dir-3	Dir-12	Dir-13	Dir-23
$V_f = 50\%$						
Maximum amplification factor	1.0	1.843 1.696	2.346 1.869	2.691 2.061	3.023 2.710	2.437 1.948
Position	All points	M2, M4, M6, M8 <i>IF2</i>	IF1 <i>M3, M7</i>	M1, M5 <i>IF2</i>	M3, M7 <i>IF1</i>	M1, M5 <i>IF2</i>
$V_f = 60\%$						
Maximum amplification factor	1.0	2.050 1.833	2.786 2.160	3.360 2.428	3.529 3.524	2.913 1.899
Position	All points	M2, M4, M6, M8 <i>IF2</i>	IF1 <i>M3, M7</i>	M1, M5 <i>IF2</i>	M3, M7 <i>IF1</i>	M1, M5 <i>M3, M7</i>
$V_f = 70\%$						
Maximum amplification factor	1.0	2.177 2.101	2.880 2.482	3.357 3.199	3.767 3.594	2.712 2.085
Position	All points	IF2 <i>M2, M4, M6, M8</i>	IF1 <i>M3, M7</i>	IF2 <i>M1, M5</i>	M3, M7 <i>IF1</i>	M1, M5 <i>M3, M7</i>

Table 5. Effect of materials on amplification factors in square array model (Figures in bold are maximum values; figures in italics are the next highest values. Positions are marked in Figure 5).

	Dir-1	Dir-2	Dir-3	Dir-12	Dir-13	Dir-23
IM7–epoxy						
Maximum amplification factor	1	2.897 2.383	2.897 2.383	4.662 4.639	4.662 4.639	2.623 2.575
Position	All points	IF1 <i>M1, M5</i>	IF2 <i>M3, M7</i>	M1, M5 <i>IF1</i>	M3, M7 <i>IF2</i>	IS <i>M1, M3, M5, M7</i>
S-glass–epoxy						
Maximum amplification factor	1	6.952 5.442	6.952 5.442	6.878 6.754	6.878 6.754	3.892 3.470
Position	All points	IF1 <i>M1, M5</i>	IF2 <i>M3, M7</i>	M1, M5 <i>IF1</i>	M3, M7 <i>IF2</i>	M1, M3, M5, M7 <i>IS</i>

elastic properties of the composite are given in Table 2. The mesh consists of 3D 20-noded isoparametric brick elements, with one element per ply in the thickness direction. One element per ply in the thickness direction is probably sufficient for modeling in-plane damage, as the following results

Table 6. Effect of materials on amplification factors in hexagonal array model (Figures in bold are maximum values; figures in italics are the next highest values. Positions are marked in Figure 5).

	Dir-1	Dir-2	Dir-3	Dir-12	Dir-13	Dir-23
IM7-epoxy						
Maximum amplification factor	1	2.050	2.786	3.360	3.529	2.913
		<i>1.833</i>	<i>2.160</i>	<i>2.428</i>	<i>3.524</i>	<i>1.899</i>
Position	All points	M2, M4, M6, M8	IF1	M1, M5	M3, M7	M1, M5
		<i>IF2</i>	<i>M3, M7</i>	<i>IF2</i>	<i>IF1</i>	<i>M3, M7</i>
S-glass-epoxy						
Maximum amplification factor	1	3.157	5.248	4.330	4.778	4.403
		<i>3.134</i>	<i>3.921</i>	<i>4.309</i>	<i>4.731</i>	<i>3.387</i>
Position	All points	M2, M4, M6, M8	IF1	M1, M5	M3, M7	M1, M5
		<i>IF</i>	<i>M3, M7</i>	<i>IF2</i>	<i>IF1</i>	<i>IF2</i>

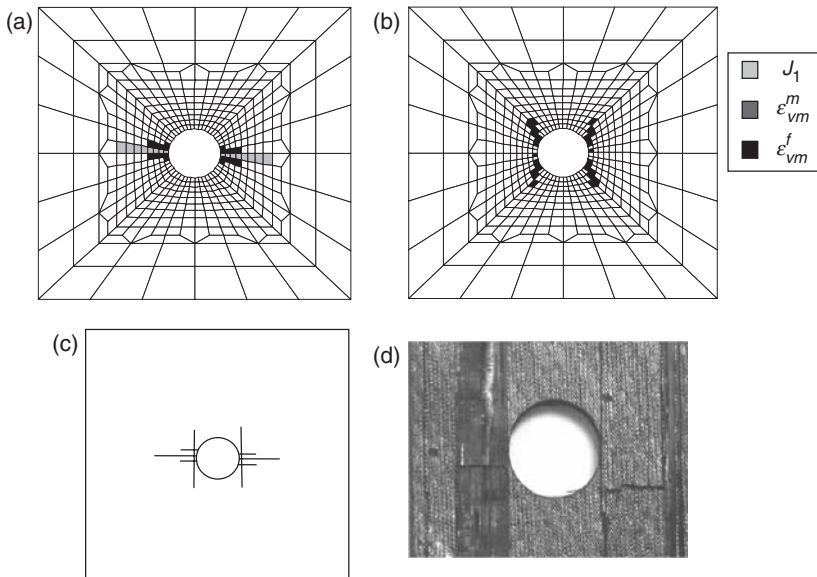


Figure 6. Damage maps for cross-ply $[0_3/90_4]_s$ laminate: (a) innermost 90° ply (sixth ply); (b) outermost 0° ply (surface ply); (c) representation by matrix cracks; and (d) damaged cross-ply specimen.

will show, but is very likely to be inadequate for modeling interlaminar stresses that lead to delamination. The nodal force modification employed is simply to zero the component of the force transverse to the fiber direction once failure is determined by SIFT. This rather simple scheme is reasonable

for initial-stage damage. Figure 6a shows the development of damage emanating from the hole edge in the innermost 90° ply. The dominant strain invariant that governs the failure of this ply is J_1 , although some elements did fail due to ε_{vm}^f . The pattern indicates that failure in the rather thick group of 90° plies is predominantly due to a large transverse crack, although other smaller transverse matrix cracks may also arise. Figure 6b shows the damage progression in the outermost 0° ply. Damage in the 0° plies appears much later than damage in the 90° plies, since the latter are weaker. The pattern suggests matrix cracking in the longitudinal direction, and a picture of a tested specimen with typical longitudinal cracks along the 0° outer ply is also shown for comparison. An alternate representation of damage, with the dominant microcracks drawn in, is shown in Figure 6c, where the damage from the 0° and 90° plies is superposed to form one diagram. This type of representation has the advantage that the damage can be more easily compared with X-ray images. A failed cross-ply specimen with typical longitudinal cracks in the surface 0° ply is shown in Figure 6d.

A word about the interpretation of local damage predicted by ε_{vm}^f may be in order here. We have already stated that the criterion ε_{vm}^f (at the locations along the fiber–matrix interface) incorporates not just the behavior of the fiber phase but also the interfacial behavior. While the superscript f denotes ‘fiber’ in the section titled ‘the stain invariant failure theory’ in the cases of damage in the 90° and 45° plies described in the preceding text, the locations where the failure by ε_{vm}^f occurred in the cases analyzed were determined to be invariably at the interface between matrix and fiber (i.e., F1–F8 in Figure 5, and never on F9). The interpretation is that the failure is mainly at the interface and not within the fiber. The same interpretation is offered if failure is located from M1–M8. However, no critical failure locations were observed on M1–M8 in all the simulations. Therefore, the failure patterns shown indicate not ‘fiber failure’ in the usual understanding of fiber breaks or splits but fiber–matrix debonding. At the ply level, the transverse cracks are assumed to traverse regions of fiber–matrix debonding and matrix cracking.

Damage maps for a laminate with a more general stacking sequence $[-45/+45/0_3/90/0]_s$ under remote uniform tensile load are shown in Figure 7. The results for the outermost -45° ply are shown in Figure 7a; when compared to the results for the $+45^\circ$ ply (Figure 7b), the former appears to suffer less damage. This suggests that stacking sequence has a significant effect on damage propagation. Both ε_{vm}^f and J_1 appear to have contributed to damage in these plies. Damage in the fifth layer is typical of a 0° ply (Figure 7c) and is dominated by ε_{vm}^f . The only 90° ply in the lay-up (Figure 7d) exhibits J_1 dominated failure; the interesting pattern suggests a distributed system of parallel transverse cracks originating from the edge

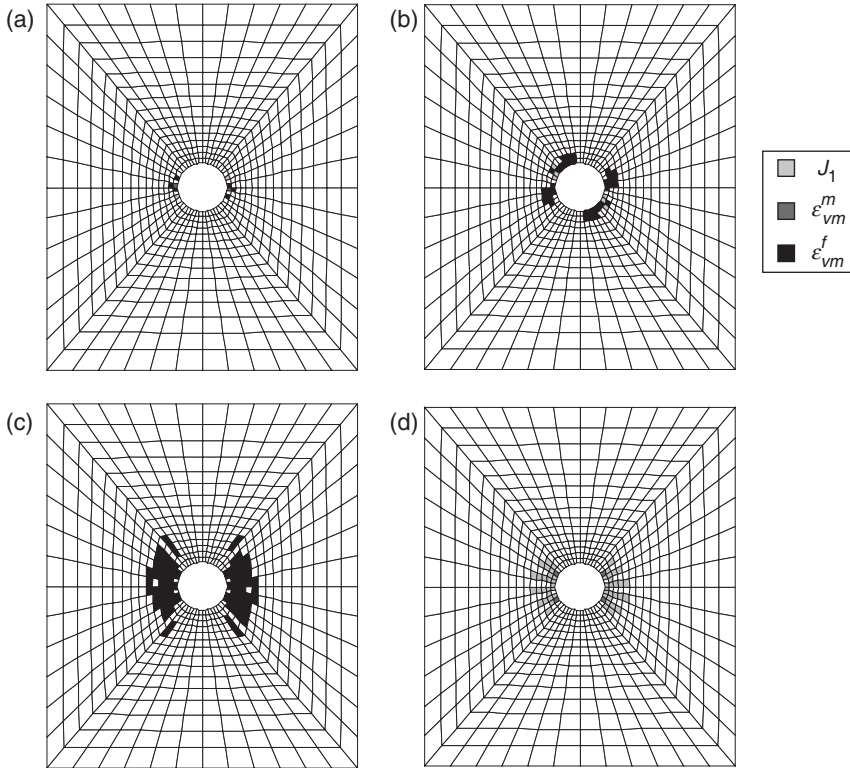


Figure 7. Damage maps for $[-45/+45/0_3/90/0]_s$ laminate: (a) -45° ply; (b) 45° ply; (c) 0° (fifth) ply; and (d) 90° ply.

of the hole. This is in contrast to the single transverse crack found in the 90° ply of the $[0_3/90_4]_s$ laminate described earlier (Figure 6a). Clearly, this difference is due to the level of constraint experienced by the 90° ply in the two laminates. It is reasonable to assume that when the level of constraint is high, as in the case of the single ply in the $[-45/+45/0_3/90/0]_s$ laminate, the damage becomes more diffused and less likely to form large single cracks. A similar analysis but with a mesh more refined around the hole is also performed, and the results shown in Figure 8. An encouraging feature is that the results do not show great sensitivity to mesh design and density. The matrix cracks representation of damage is shown in Figure 9. It shows a reasonable distribution of damage that may be expected from an OHT specimen.

The foregoing analysis was performed without consideration for delamination in order to save computational effort. It was, therefore,

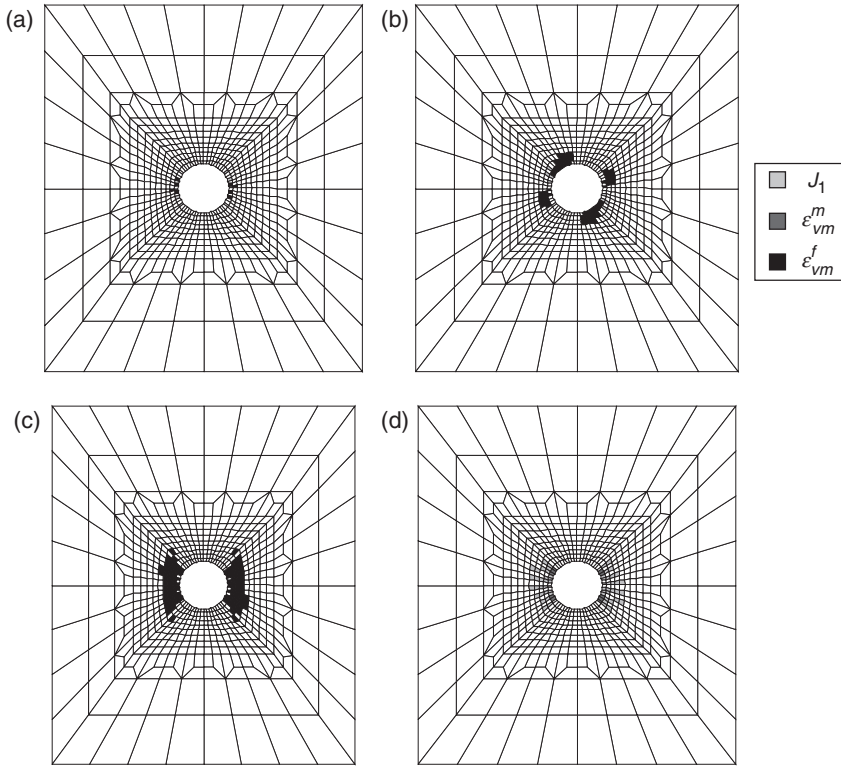


Figure 8. Damage maps for $[-45/+45/0_3/90/0]_s$ laminate (refined mesh around hole): (a) -45° ply; (b) 45° (fifth) ply; (c) 0° ply; and (d) 90° ply.

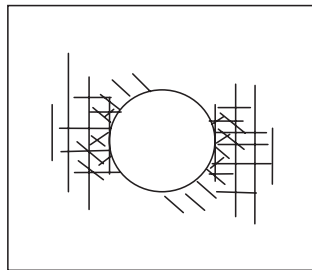


Figure 9. Matrix cracks representation for the $[-45/+45/0_3/90/0]_s$ laminate.

decided to analyze two cases of OHT specimens with three elements per ply in the thickness direction and to apply nodal force modification to the out-of-plane force components when failure is determined by SIFT. The out-of-plane modification of nodal forces is applied only to failed elements adjacent

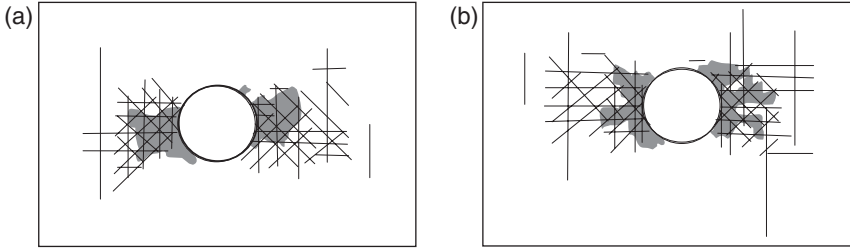


Figure 10. Predicted matrix cracks and delaminations for: (a) $[45/0/-45/90]_s$ and (b) $[\pm 45/90/0]_s$ laminates.

to the relevant interface between plies of different fiber orientations. For example, if possible delamination is allowed between the 45° and 0° plies, the failed elements on either side of the interface between the two plies will have their nodal forces modified in the thickness direction, in addition to modification of in-plane nodal forces. It was found that this scheme may result in rather large out-of-plane strains, i.e., ϵ_{33} , γ_{13} , and γ_{23} , very close to the edge of the hole. The in-plane strains, however, remain relatively small. In this way, it is possible to map out potential areas of delamination for each interface between plies of dissimilar fiber orientations. The superimposed delaminations from each interface may be combined with predicted system of transverse crack to form composite images. Two quasi-isotropic laminates with different stacking sequences ($[45/0/-45/90]_s$ and $[\pm 45/90/0]_s$) are analyzed, and the combined damage and delamination maps are shown in Figure 10. The predicted ultimate failure loads are 474.4 MPa (68.8 ksi) for the $[45/0/-45/90]_s$ laminate and 518.5 MPa (75.2 ksi) for the $[\pm 45/90/0]_s$ laminate. These values are in reasonable agreement with the experimental results of 413.7 MPa (60 ksi) for the $[45/0/-45/90]_s$ laminate and 556.4 MPa (80.7 ksi) for the $[\pm 45/90/0]_s$ laminate (Kim and Sihm, 2004). The lower ultimate strength for the $[45/0/-45/90]_s$ laminate is correctly predicted by the analysis. It appears that nodal force modification in the through thickness direction is necessary to correctly account for the interlaminar effects of changing the stacking sequence, although it does not affect the in-plane damage patterns significantly. However, in order to predict delamination, at least three elements per ply in the thickness direction is necessary, which considerably increases the computational effort. The authors are developing submodeling techniques so that local damage and delamination patterns close to regions of high stress gradients may be predicted using 3D SIFT-EFM, while the rest of the structure may be modeled using shell or plate elements. This approach will enable modeling of damage progression in practical structures with more reasonable resources, but will have the

disadvantage that the damage cannot be simulated beyond the zone of the 3D elements.

CONCLUSION

The element-failure or nodal force modification method is introduced for the modeling of damage in composite laminates. It assumes that the deleterious effects of damage on mechanical properties can be effectively modeled through the manipulation of nodal forces, which are then applied to the FE as damage progresses. The method has the advantage that no elements are removed from the FE mesh, and therefore, it has a mechanism to ensure that interpenetration of crack surfaces does not occur. Furthermore, the material stiffness properties are not altered, ensuring that no recalculation of FE stiffness matrices is necessary. This is in contrast to conventional material property degradation techniques, which may result in computational problems because convergence is not always assured and results may be highly mesh-dependent. The EFM has been applied in this study with a recent micromechanics-based composite SIFT to predict damage pattern evolution for open-hole tension problems. This combined SIFT-EFM approach appears to predict reasonable damage patterns emanating from a hole in laminates loaded under remote tension. Furthermore, the results are independent of mesh design and density.

ACKNOWLEDGMENT

Partial support for this research was provided by the US Air Force Office for Scientific Research.

REFERENCES

- Beissel, S.R., Johnson, G.R. and Popelar, C.H. (1998). An Element-failure Algorithm for Dynamic Crack Propagation in General Directions, *Engineering Fracture Mechanics*, **61**(3-4): 407-425.
- Camanho, P.P. and Matthews, F.L. (1999). A Progressive Damage Model for Mechanically Fastened Joints in Composite Laminates, *Jour. Composite Mater.*, **33**(24): 2248-2279.
- Cheng, M. and Chen, W. (2006). Modeling Transverse Behavior of Kevlar KM2 Single Fibers with Deformation-induced Damage, *Int. Jour. Damage Mechanics*, **15**(2): 121-132.
- Chow, C.L., Yang, F. and Asundi, A. (1993). A Three-dimensional Analysis of Symmetric Composite Laminates with Damage, *Int. Jour. Damage Mechanics*, **2**: 229-245.
- Gibson, R.F. (1994). *Principles of Composite Material Mechanics*, McGraw-Hill, Inc., New York, USA.
- Gosse, J.H. and Christensen, S. (2001). Strain Invariant Failure Criteria for Polymers in Composite Materials, *AIAA-2001-1184*.

- Gosse, J.H. (2002). An Overview of Strain Invariant Failure Theory (SIFT), In: Chang, F.-K. (ed.), *Proc. 10th US-Japan Conference on Composite Materials*, 16–18 September, Stanford, US, pp. 989–997, DEStech Publications, US.
- Ha, S.K. (2002). Micromechanics in the Analysis of Composite Structures, *6th Composites Durability Workshop (CDW-6)*, Tokyo, Japan, 14–15 November.
- Jin, K.K., Oh, J.H. and Ha, S.K. (2007). Effect of Fiber Arrangement on Residual Thermal Stress Distributions in a Unidirectional Composite, *Jour. Composite Materials* **41**(5): 591–611.
- Ju, J.W., Ko, Y.F. and Ruan, H.N. (2006). Effective Elastoplastic Damage Mechanics for Fiber-reinforced Composites with Evolutionary Complete Fiber Debonding, *Int. Jour. Damage Mechanics*, **15**(3): 237–265.
- Kim, R. and Sihm, S. (2004). Effects of Stacking Sequence, *9th Composites Durability Workshop (CDW-9)*, Shanghai, China, 1–2 November.
- Kim, Y., Davalos, J.F. and Barbero, E.J. (1996). Progressive Failure Analysis of Laminated Composite Beams, *Jour. Composite Materials*, **30**(5): 536–560.
- Kollar, L.P. and Springer, G.S. (2003). *Mechanics of Composite Structures*, Cambridge University Press, Cambridge, UK.
- Mahishi, J.M. (1986). An Integrated Micromechanical and Macromechanical Approach to Fracture Behavior of Fiber-reinforced Composites, *Engineering Fracture Mechanics*, **25**(2): 197–228.
- Mayes, J.S. and Hansen, A.C. (2001). Multicontinuum Failure Analysis of Composite Structural Laminates, *Mechanics of Composite Materials and Structures*, **8**(4): 249–262.
- Ochoa, O.O. and Engblom, J.J. (1987). Analysis of Progressive Failure in Composites, *Composites Science & Technology*, **28**(2): 87–102.
- Paulino, G.H., Yin, H.M. and Sun, L.Z. (2006). Micromechanics-based Interfacial Debonding Model for Damage of Functionally Graded Materials with Particle Interactions, *Int. Jour. Damage Mechanics*, **15**(3): 267–288.
- Shokrieh, M.M. and Lessard, L.B. (2000). Progressive Fatigue Damage Modeling of Composite Materials, Part I: Modeling, *Jour. Composite Mater.*, **34**(13): 1056–1079.
- Talreja, R. (1994). Damage Characterization by Internal Variables, In: Talreja, R. (ed.), *Damage Mechanics of Composite Materials*, pp. 53–78, Elsevier Science, Amsterdam, The Netherlands.
- Tay, T.E. (2003). Characterization and Analysis of Delamination Fracture in Composites – An Overview of Developments from 1990 to 2001, *Appl. Mech. Revs.*, **56**(1): 1–32.
- Tay, T.E., Tan, V.B.C. and Deng, M. (2003). Element-failure Concepts for Dynamic Fracture and Delamination in Low-velocity Impact of Composites, *Int. Jour. of Solids & Structures*, **40**(3): 555–571.
- Tay, T.E., Tan, V.B.C. and Tan, S.H.N. (2005). Element-failure: An Alternative to the Material Property Degradation Method for Progressive Damage in Composite Structures, *Jour. of Composite Materials*, **39**(18): 1659–1675.
- Tsai, S.W. (1992). *Theory of Composites Design*, *Think Composites*, Dayton, USA.
- Tserpes, K.I., Papanikos, P. and Kermanidis, T. (2001). A Three-dimensional Progressive Damage Model for Bolted Joints in Composite Laminates Subjected to Tensile Loading, *Fatigue Fract. Engng. Mater. Struct.*, **24**(10): 663–675.
- Wolford, G.F. and Hyer, M.W. (2005). Failure Initiation and Progression in Internally-pressurized Elliptical Composite Cylinders, *Mechanics of Advanced Materials and Structures*, **12**(6): 437–455.
- Yee, J.C.H. and Pellegrino, S. (2005). Folding of Woven Composite Structures, *Composites Part A: Applied Science & Manufacturing*, **36**(2): 273–278.